Chemical Science

ROYAL SOCIETY OF CHEMISTRY

EDGE ARTICLE

View Article Online
View Journal | View Issue

Check for updates

Cite this: *Chem. Sci.*, 2025, **16**, 9820

All publication charges for this article have been paid for by the Royal Society of Chemistry

Received 7th November 2024
Accepted 13th April 2025

DOI: 10.1039/d4sc07559e

rsc.li/chemical-science

Open Access Article. Published on 24 April 2025. Downloaded on 2/22/2026 5:57:45 PM. This article is licensed under a Creative Commons Attribution-NonCommercial 3.0 Unported Licence.

Multi-site reduction of hexachlorophosphazene to low-valent PN heterocycles and extension to the reduction of poly-chlorophosphazene†

Etienne A. LaPierre, *[a] Roope A. Suvinen, [b] Brian O. Patrick, [c] Heikki M. Tuononen *[b] and Ian Manners ‡[a]

Facile one and two site reduction of hexachlorophosphazene using cyclic (alkyl)(amino)carbene substituents are shown to yield *P*-CAAC^{Me}-*cyclo*-(PNP(Cl)$_2$NP(Cl)$_2$N) **1** and *P*,*P*′-bis-CAAC^{Me}-*cyclo*-(PNPNP(Cl)$_2$N) **2** (CAAC^{Me} = 1-[2,6-bis(isopropyl)phenyl]-3,3,5,5-tetramethyl-2-pyrrolidinylidene), respectively. Compound **1** is characterized by its predominantly phosphorus-centered HOMO, which results in typical phosphine-type nucleophilic and reductive reactivity; however, the resultant compounds of such reactions feature properties distinct from their classical phosphine analogues due to the CAAC-centered LUMO, which acts as an acceptor for both intramolecular interactions and photophysical excitations. In contrast, compound **2** exhibits π-conjugation spanning the endocyclic PNP moiety and the two CAAC^{Me} substituents, despite its non-planar structure. Treatment of **2** with [Cp*RuCl]$_4$ results in the electrophilic displacement of one of the CAAC^{Me} moieties by two Cp*RuCl fragments to yield the spirocyclic compound **3**. Preliminary results show that the methodology used to reduce hexachlorophosphazene to **1** can be directly transposed to the regiospecific reduction of poly-chlorophosphazene, to yield poly-**1**, a fundamentally new class of inorganic polymer that possesses a phosphorus center with chemically active lone pairs in the main chain.

Introduction

First identified by von Liebig in 1834 as a product of the condensation of PCl_5 with ammonia,[1] hexachlorophosphazene, *cyclo*-$(NPCl_2)_3$, has attracted significant interest, both due to its unusual bonding and chemical properties as well as its practical utility in synthesis. Hexachlorophosphazene is notable for its planar structure, uniform bond lengths and angles, and resistance to hydrolysis by ambient moisture typical of chlorophosphoranes. While these properties were originally attributed to aromaticity arising from π-bonding invoking phosphorus d-orbitals,[2] it is now widely accepted that phosphazenes do not exhibit such π-bonding, and these features arise instead from the negative hyperconjugation of the nitrogen-centered lone pair into phosphorus-chlorine σ* orbitals.[3–5] The early chemistry of hexachlorophosphazene was meticulously investigated by Stokes in the 1890s,[6–8] who noted the formation of a hydrolytically sensitive "inorganic rubber", poly-chlorophosphazene, upon thermolysis. This material remained a curiosity due to its sensitivity until reports by Allcock and coworkers in the 1960s demonstrated the facile derivatization of the polymer chain by nucleophilic substitution of the phosphorus–chloride bonds to yield air and moisture stable high polymers.[9,10] This process has been expanded to a wide variety of nucleophiles resulting in poly-phosphazenes with a broad range of properties and potential applications.[11–17] In addition to its use as a polymer precursor, hexachlorophosphazene also possesses rich substitution chemistry,[18] which has been utilized for the synthesis of numerous derivatives, notably well-defined phosphazene dendrimers.[19,20]

In contrast to the well-developed polymerization and substitution chemistry, development of the controlled reduction chemistry of hexachlorophosphazene consists of a single example by Rivard and coworkers,[21] whereby a single phosphorus center can be reduced in the presence of a stabilizing N-heterocyclic carbene (NHC) to compound **A** (Chart 1). Likewise, the reduction chemistry of the fluorine congener, hexafluorophosphazene, which is known to give more predictable reactivity with organometallic reagents, is similarly scant, being limited to single site reduction by formal reductive metalation using transition metal carbonyl derivatives, giving compounds

[a]*Department of Chemistry, University of Victoria, 3800 Finnerty Rd, Victoria, British Columbia, V8P 5C2, Canada. E-mail: elapierre@uvic.ca*

[b]*Department of Chemistry, NanoScience Centre, University of Jyväskylä, P. O. Box 35, FI-40014 Jyväskylä, Finland. E-mail: heikki.m.tuononen@jyu.fi*

[c]*Department of Chemistry, University of British Columbia, 2036 Main Mall, Vancouver, British Columbia, V6T 1Z1, Canada*

† Electronic supplementary information (ESI) available. CCDC 2383407–2383415. For ESI and crystallographic data in CIF or other electronic format see DOI: https://doi.org/10.1039/d4sc07559e

‡ Ian Manners: deceased December 3rd, 2023.

© 2025 The Author(s). Published by the Royal Society of Chemistry

Open Access Article. Published on 24 April 2025. Downloaded on 2/22/2026 5:57:45 PM.
This article is licensed under a Creative Commons Attribution-NonCommercial 3.0 Unported Licence.

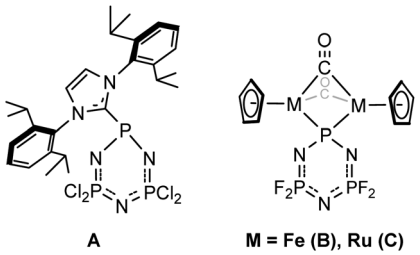

Chart 1 Examples of reduced cyclic six-membered phosphazene rings.

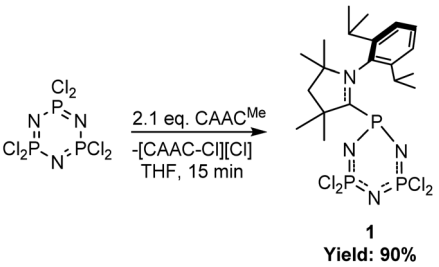

Scheme 1 Reduction and ligation of hexachlorophosphazene by $CAAC^{Me}$ to yield **1**.

B and **C** (Chart 1). However, even formal reduction in these cases is questionable given the ambiguity in oxidation state of the metal centers.[15,22–24] Recently, we have explored the controlled reduction of linear chlorophosphazenes to give formally low-valent PN compounds stabilized by the cyclic (alkyl)(amino)carbene[25] 1-[2,6-bis(isopropyl)phenyl]-3,3,5,5-tetramethyl-2-pyrrolidinylidene ($CAAC^{Me}$).[26,27] Notably, such species were found to exhibit delocalized π-bonding and share an isoelectronic relationship with conjugated hydrocarbons, unlike their high-valent analogues, as well as a rich-redox chemistry. Given these results, the general superiority of CAAC ligands in stabilizing low-valent species compared to NHCs,[28–30] and the paucity of low-valent PN compounds,[31–37] despite wide-spread interest,[38–48] the suitability of CAACs for stabilizing the reduction products of hexachlorophosphazene, particularly in order to access cyclic conjugated species, such as *cyclo*-$(PN)_3$, warrants investigation.

Results and discussion

Synthesis and structure of 1

Firstly, the direct reaction of $CAAC^{Me}$ with hexachlorophosphazene was explored in the absence of external reducing agents.[26,49] Reaction of these compounds in a 1 : 1 ratio led to immediate salt formation and development of a bright orange solution. Subsequent analysis by $^{31}P\{^1H\}$ NMR spectrometry revealed the consumption of one-half of hexachlorophosphazene and formation of a new AX_2 spin system with $\delta_P = 104.3$ (A) and 4.6 ppm (X), and a coupling constant of 87 Hz, consistent with the reduction of a single phosphorus center by two equivalents of $CAAC^{Me}$ and concomitant formation of [CAAC–Cl][Cl] as a by-product. Accordingly, addition of a further equivalent of $CAAC^{Me}$ resulted in full consumption of hexachlorophosphazene and complete and quantitative conversion to the novel orange product **1** (Scheme 1). This is in contrast to reports by Rivard and coworkers,[21] where the lack of a strong external reductant, such as sodium metal, gave mixtures of products and only trace conversion to the desired reduction product, a difference likely arising due to the superior reducing power of $CAAC^{Me}$ relative to NHCs.[26,29,49]

The room temperature ^1H NMR spectrum of **1** in C_6D_6 shows apparent C_s symmetry, featuring a single set of resonances corresponding to the $CAAC^{Me}$ substituent. Similarly, the solid-state structure of **1**, determined by single crystal X-ray diffraction studies, is approximately C_s symmetric (Fig. 1) with only minor puckering of the $CAAC^{Me}$ ring. Density functional theory (DFT) calculations at the PBE0-GD3BJ/def2-TZVP level[50–52] showed that the Gibbs free energy of activation for the $CAAC^{Me}$ ring flip is only 3.33 kcal mol^{-1}. As the barriers associated with the rotation of the $CAAC^{Me}$ moiety are also small (*vide infra*), rapid interconversion between different conformers takes place, leading to spectroscopic data consistent with pseudo-C_s symmetry.

The $CAAC^{Me}$ ligated phosphorus atom in **1** is bent away from the plane of the phosphazene ring, exhibiting pyramidalized geometry ($\Sigma = 303.91°$) and a long P–C bond length of 1.912(1) Å, longer than that found in **A** (1.8791(13) Å).[21] The latter feature may be explained by the orthogonal disposition of the formally vacant orbital of the carbene carbon to the lone pair at phosphorus that prevents back-donation, an assertion supported by natural bond orbital (NBO) analyses that showed no significant donor–acceptor interactions between these orbitals. Further, the P–N bond lengths between the reduced phosphorus center and the adjacent nitrogen atoms are significantly elongated in **1** with respect to those in hexachlorophosphazene (1.6793(9) Å *vs.* 1.577(3) Å),[53] while the P–N bond lengths between the nitrogen centers adjacent to the reduced phosphorus center and the PCl_2

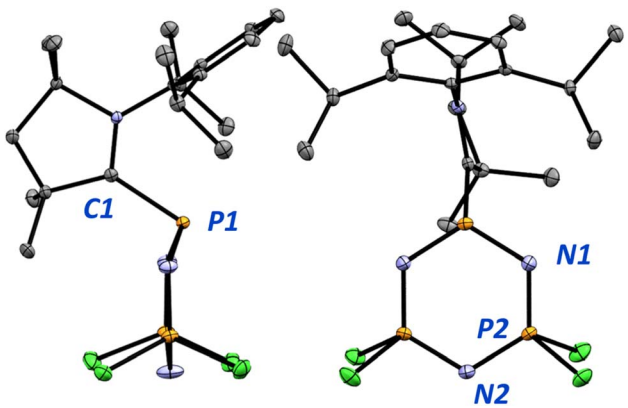

Fig. 1 Molecular structure of **1** shown from two perspectives. Ellipsoids are drawn at 50% probability. Hydrogen atoms are omitted for clarity. Select bond lengths (Å) and angles (°) for **1** [calculated values in square brackets]: P1–C1 1.912(1) [1.904]; C1–N4 1.301(2) [1.291]; P1–N1 1.6793(9) [1.665]; N1–P2 1.546(1) [1.553]; P2–N2 1.593(1) [1.588]; C1–P1–N1 98.14(5) [100.1]; N1–P1–N3 108.50(6) [109.3].

Open Access Article. Published on 24 April 2025. Downloaded on 2/22/2026 5:57:45 PM. This article is licensed under a Creative Commons Attribution-NonCommercial 3.0 Unported Licence.

fragments are contracted. The former may be rationalized by reduced electrostatic attraction and lack of negative hyperconjugation, while the latter is likely due to increased negative hyperconjugation from the more electron rich nitrogen centers to the P–Cl σ* orbitals.

As most phosphorus(III) compounds, such as **A**, are colorless or weakly colored, we sought to investigate the reason for the striking orange coloration of **1**. Analysis of **1** by UV-Vis spectrometry in THF (Fig. S1†) revealed a strong transition with λ_{max} = 438 nm ($\varepsilon_{438} = 4.65 \times 10^3$ M^{-1} cm^{-1}), while similar analysis in toluene (Fig. S2†) showed the absorption properties of **1** to be solvent dependent, with a slight red-shifting of the absorption maximum (λ_{max} = 442 nm) and a dramatic increase in the extinction coefficient ($\varepsilon_{442} = 8.11 \times 10^3$ M^{-1} cm^{-1}). Further, time-dependent density functional theory (TD-DFT) calculations employing implicit solvation for THF or toluene (polarizable continuum model using the integral equation formalism variant, IEFPCM)[54] indicated that **1** should lack meaningful transitions in the visible light region, with an exceptionally weak oscillator strength ($f = 0.0001$) calculated for the $S^0 \rightarrow S^1$ HOMO to LUMO transition at around 500 nm. This agrees with the orthogonal orientation of the predominantly phosphorus lone pair HOMO and the carbene-centered C–N π* LUMO (Fig. 2), which prevents effective overlap between donor and acceptor orbitals. With this in mind, alternative energetically accessible conformations of **1** that better agree with the observed photophysical behavior were explored computationally.

A relaxed potential energy scan of the rotation of the CAAC moiety about the P–C bond in **1** identified several additional minima. Of lowest energy is $\mathbf{1}_{C1}$ with the CAAC^{Me} moiety rotated *ca.* 90° about the P–C bond axis relative to the pseudo-C_s symmetric structure, denoted hereafter $\mathbf{1}_{Cs}$ (Fig. 2 and S3†). Interestingly, the asymmetric rotamer $\mathbf{1}_{C1}$ is 4.55 kcal mol^{-1} lower in Gibbs free energy than the experimentally observed structure $\mathbf{1}_{Cs}$ and has a significantly shorter P–C bond; 1.790 Å in $\mathbf{1}_{C1}$ compared to 1.904 Å in $\mathbf{1}_{Cs}$. Accordingly, the frontier Kohn–Sham orbitals of $\mathbf{1}_{C1}$ are distinct from those of $\mathbf{1}_{Cs}$ (Fig. 2), with the HOMO and LUMO of $\mathbf{1}_{C1}$ being the in-phase and out-of-phase combinations of the phosphorus lone pair and the C–N π* orbital, respectively. Consequently, the HOMO of $\mathbf{1}_{C1}$ is lower in energy by *ca.* 0.1 eV compared to $\mathbf{1}_{Cs}$, while the LUMO is similarly destabilized. NBO analyses showed a markedly increased Wiberg bond index[55] for the P–C bond in $\mathbf{1}_{C1}$ *vs.* $\mathbf{1}_{Cs}$ (1.15 *vs.* 0.78), likely arising from the significant donor–acceptor interaction (53.05 kcal mol^{-1}) between the phosphorus lone-pair and the C–N π* orbital in $\mathbf{1}_{C1}$.

TD-DFT calculations for $\mathbf{1}_{C1}$ using implicit solvation for THF revealed a strong ($f = 0.154$) electronic transition at 410 nm arising from the $S^0 \rightarrow S^1$ HOMO to LUMO excitation, in good agreement with the experiments. Performing the calculations using implicit toluene solvation *in lieu* of THF accurately reproduces the slight red-shifting of the absorption maximum observed (416 nm), though the difference in the computed oscillator strength ($f = 0.171$) does not explain the difference in the observed absorptivity in these solvents. Consequently, the energy difference between the two rotamers in different environments was computed, revealing a greater preference for $\mathbf{1}_{C1}$ in the gas phase (−4.55 kcal mol^{-1}) or toluene (−3.37 kcal mol^{-1}) than in THF (−2.30 kcal mol^{-1}), which follows the experimental solvent dependence in absorptivity. Presumably, the preference for **1** to crystallize as $\mathbf{1}_{Cs}$ over the lower energy rotamer $\mathbf{1}_{C1}$ arises from solid-state packing effects combined with the ease of $\mathbf{1}_{Cs} \rightarrow \mathbf{1}_{C1}$ interconversion that has a calculated Gibbs free energy of activation of only 4.15 kcal-mol^{-1} in the gas phase; the calculated Gibbs free energy of activation for the reverse process $\mathbf{1}_{C1} \rightarrow \mathbf{1}_{Cs}$ is 8.70 kcal mol^{-1}.

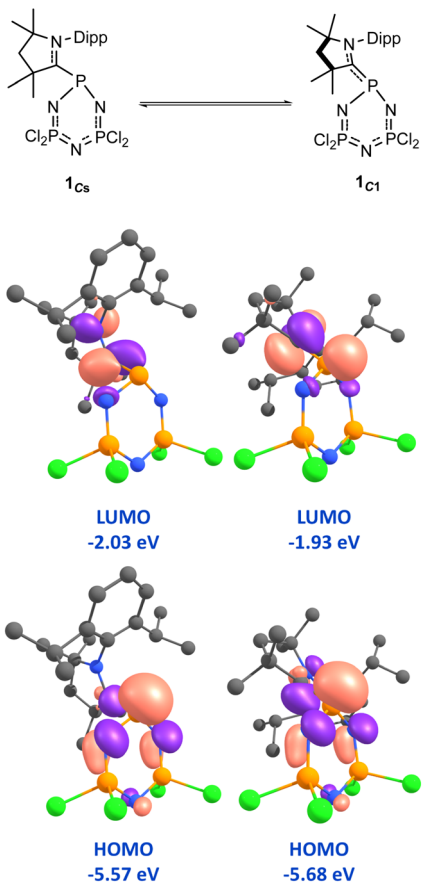

Fig. 2 Frontier Kohn–Sham orbitals of two rotamers of **1** with pseudo-C_s (left, $\mathbf{1}_{Cs}$) and C_1 (right, $\mathbf{1}_{C1}$) symmetry (isovalue = ±0.06 a.u.). Dipp = 2,6-diisopropylphenyl.

Oxidation and metalation of 1

With the HOMO of **1** being predominantly phosphorus lone pair in nature (Fig. 2), the ability of **1** to engage in archetypical phosphine reactivity was explored. As **A** was previously demonstrated to react with elemental sulfur to yield a formal phosphine sulfide, we explored the reactivity of **1** with various chalcogen transfer reagents (Scheme 2). This showed that **1** reacts with oxygen, sulfur, or selenium transfer reagents to generate the corresponding phosphorus chalcogenides $\mathbf{1}_{Ch}$ (Ch = O, S, or Se) in high yield. Compound $\mathbf{1}_{O}$ is colorless, with room temperature ^{1}H and ^{31}P{H} NMR spectra in $CDCl_3$ consistent with pseudo-C_s symmetry. Notably, the ^{31}P NMR

© 2025 The Author(s). Published by the Royal Society of Chemistry

Open Access Article. Published on 24 April 2025. Downloaded on 2/22/2026 5:57:45 PM. This article is licensed under a Creative Commons Attribution-NonCommercial 3.0 Unported Licence.

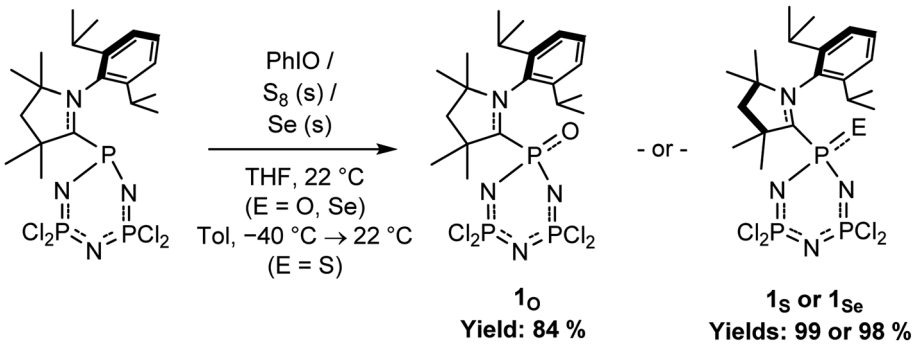

Scheme 2 Chalcogenation of **1** by PhIO or elemental chalcogens.

resonance corresponding to the oxidized phosphorus center is shifted dramatically upfield to $\delta_P = -16.0$ ppm, in contrast to organophosphines that typically shift downfield. The $^{31}P\{^1H\}$ NMR spectra of $\mathbf{1_S}$ and $\mathbf{1_{Se}}$ likewise feature a smaller upfield shift of the resonance corresponding to the oxidized phosphorus center, which in $\mathbf{1_{Se}}$ also shows distinct satellites (J = 710 Hz) with an area (7 : 93) consistent with ^{77}Se coupling;[56] correspondingly, the ^{77}Se NMR spectrum of $\mathbf{1_{Se}}$ consists of a doublet at $\delta_{Se} = 215.7$ ppm. While the magnitude of the $^1J_{P-Se}$ coupling constant has been used to evaluate the bonding in phosphine selenides,[57] the presence of confounding intramolecular interactions in $\mathbf{1_{Se}}$ (*vide infra*), which have been shown to influence the coupling constant and ^{77}Se NMR chemical shift in phosphine[58] and related carbene selenides,[59] preclude such analysis. Saliently, the resonances for the PCl_2 centers in the $^{31}P\{^1H\}$ NMR spectrum of both $\mathbf{1_S}$ and $\mathbf{1_{Se}}$ are broadened, indicative of inequivalent sites in dynamic exchange. The ^{1}H NMR spectra of $\mathbf{1_S}$ and $\mathbf{1_{Se}}$ are similarly broadened, indicative of dynamic exchange and consistent with hindered rotation about the C–P bond. In further contrast with $\mathbf{1_O}$, both $\mathbf{1_S}$ and $\mathbf{1_{Se}}$ are colored, the former yellow and the latter orange.

The solid-state structures of all compounds in the series $\mathbf{1_{Ch}}$ were examined by X-ray crystallography. Unfortunately, single crystals of $\mathbf{1_O}$ of suitable quality for full analysis could not be obtained; however, connectivity could be established (Fig. S4†), which indicates that $\mathbf{1_O}$ crystallizes with approximate C_s symmetry, similarly to **1**. In contrast, the structures of the heavier congeners $\mathbf{1_S}$ and $\mathbf{1_{Se}}$ show the CAAC^{Me} moiety to be rotated by *ca.* 90° about the P–C bond (Fig. 3), similarly to the calculated structure $\mathbf{1_{C1}}$. The P–Ch distances are comparable to those in respective triphenylphosphine analogues (1.9487(6) *vs.* 1.950(3) Å (ref. 60) and 2.096(2) *vs.* 2.106(1) Å (ref. 61) for S and Se, respectively). In both $\mathbf{1_S}$ and $\mathbf{1_{Se}}$, the C–P–Ch bond angle is narrowed considerably from idealized tetrahedral geometry (∠C–P–S = 99.13(6)°, ∠C–P–Se = 98.2(2)°), in contrast to sulfurized **A** (Chart 1), which features a more typical C–P–S angle of 105.02(6).[21] Given the orientation of the CAAC^{Me} fragment, these relatively acute angles suggest an interaction between the heavy chalcogen and the formally vacant orbital on carbon. The C···Ch distances are 2.898(2) and 2.990(5) Å for S and Se, respectively, both significantly shorter than sum of van der Waals radii for the corresponding elements.

Analysis of the calculated Kohn–Sham frontier orbitals for both $\mathbf{1_S}$ and $\mathbf{1_{Se}}$ showed that the HOMO−1 and the LUMO correspond to the in-phase and out-of-phase combinations of a chalcogen lone pair and the C–N π* orbital, respectively, while the HOMO is another lone pair on the chalcogen element (Fig. 4). NBO analyses revealed sizeable through-space C···Ch donor–acceptor interactions in both $\mathbf{1_S}$ and $\mathbf{1_{Se}}$ (14.08 and 13.95 kcal mol^{-1}, respectively), which, combined with the steric profile imposed by the large chalcogen atom, provide a rationale for restricted rotation about the P–C bond observed by NMR spectrometry (*vide supra*). Further, the presence of this interaction explains the unexpected coloration of both compounds. The UV-Vis spectra of $\mathbf{1_S}$ and $\mathbf{1_{Se}}$ in THF feature strong absorptions at 340 nm ($\varepsilon_{340} = 4.52 \times 10^3$ M^{-1} cm^{-1}) and 387 nm ($\varepsilon_{387} = 5.34 \times 10^3$ M^{-1} cm^{-1}), respectively, that TD-DFT calculations with implicit THF solvation suggest to arise from $S^0 \rightarrow S^2$ transitions of primarily HOMO−1 to LUMO character.

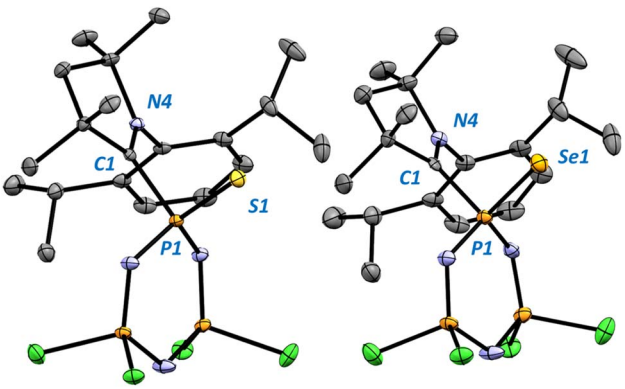

Fig. 3 Molecular structures of $\mathbf{1_S}$ (left) and $\mathbf{1_{Se}}$ (right). Ellipsoids are drawn at 50% probability. Hydrogen atoms are omitted for clarity. Select bond lengths (Å) and angles (°) for $\mathbf{1_S}$: P1–C1 1.858(2) [1.833]; P1–S1 1.82965 [1.947]; C1–N4 1.305(2) [1.303]; P1–N1 1.625(1) [1.613]; N1–P2 1.558(2) [1.561]; P2–N2 1.591(2) [1.585]; C1–P1–S1 99.13(6) [94.4]; C1–P1–N1 108.60(8) [108.4]; N1–P1–N3 111.42(8) [112.7]. Select bond lengths (Å) and angles (°) for $\mathbf{1_{Se}}$: P1–C1 1.850(5) [1.830]; P1–Se1 2.098(2) [2.103]; C1–N4 1.306(7) [1.307]; P1–N1 1.613(4) [1.612]; N1–P2 1.556(5) [1.563]; P2–N2 1.580(5) [1.584]; C1–P1–Se1 98.2(2) [94.4]; C1–P1–N1 109.2(2) [108.4]; N1–P1–N3 111.7(2) [113.1].

Open Access Article. Published on 24 April 2025. Downloaded on 2/22/2026 5:57:45 PM. This article is licensed under a Creative Commons Attribution-NonCommercial 3.0 Unported Licence.

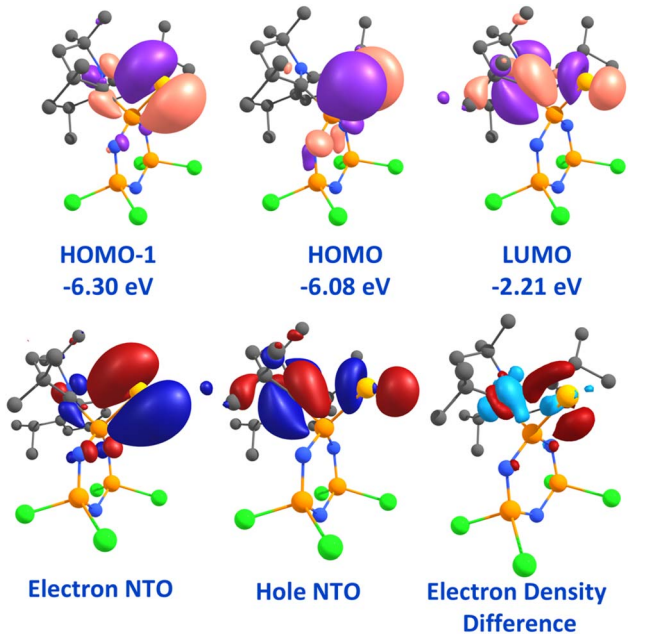

Fig. 4 Top: Frontier Kohn–Sham molecular orbitals of $\mathbf{1_{Se}}$ (isovalue = ±0.04 a.u.). Bottom: Natural transition orbitals (NTOs; isovalue = ±0.04 a.u.) and the electron density difference map (isovalue = ±0.006 a.u.; red = depletion, teal = accumulation) for the $S^0 \rightarrow S^2$ transition of $\mathbf{1_{Se}}$. The orbitals of $\mathbf{1_S}$ are qualitatively similar.

The solution dynamics of $\mathbf{1_S}$ and $\mathbf{1_{Se}}$ were further explored by variable temperature NMR spectrometry in $CDCl_3$. At 213 K, both $\mathbf{1_S}$ and $\mathbf{1_{Se}}$ exhibit $^{31}P\{^1H\}$ and ^1H NMR spectra that are consistent with C_1 symmetry and show no evident line broadening, indicative of the existence of a single conformer at this temperature (Fig. S5–S8†); in contrast, $\mathbf{1_O}$ shows spectra consistent with a pseudo-C_s symmetric structure at the same temperature (Fig. S9 and S10†). For both $\mathbf{1_S}$ and $\mathbf{1_{Se}}$, ^1H NMR spectra were acquired at temperatures between 273 and 313 K and modelled to extract rate constants *via* line shape analysis. Eyring analysis (Fig. S11 and S12†) reveals positive enthalpies of activation for bond rotation, $\Delta H^{\ddagger} = 9.69 \pm 0.17$ and 9.50 ± 0.36 kcal mol^{-1} for $\mathbf{1_S}$ and $\mathbf{1_{Se}}$, respectively, with significant negative entropies of activation, $\Delta S^{\ddagger} = -9.56 \pm 0.60$ and -12.9 ± 1.21 cal K^{-1} mol^{-1} for $\mathbf{1_S}$ and $\mathbf{1_{Se}}$, respectively, indicative of an ordered transition state in both cases. DFT analysis of the rotation of the CAAC moiety about the P–C bond in $\mathbf{1_{Ch}}$ with implicit solvation model for $CDCl_3$ gave $\Delta H^{\ddagger}$ (at 298 K and 1 atm) of 7.48, 12.42, and 13.78 kcal mol^{-1} for the $C_1 \rightarrow C_s$ interconversion of $\mathbf{1_O}$, $\mathbf{1_S}$, and $\mathbf{1_{Se}}$, respectively; calculated enthalpies of activation for the reverse rotation $C_s \rightarrow C_1$ are 6.39, 7.61, and 7.93 kcal mol^{-1}, respectively. The DFT data show the expected trend and suggest largely unhindered rotation about the P–C bond for $\mathbf{1_O}$ at 213 K, while the same rotation in $\mathbf{1_S}$ and $\mathbf{1_{Se}}$ is clearly restricted with almost twice the barrier height. Interestingly, the calculated entropies of activation are negative but negligible for all compounds $\mathbf{1_{Ch}}$, suggesting that explicit interactions with solvent molecules play a large role in modulating the entropies.

The properties of **1** as a ligand in transition metal complexes was explored by the synthesis of analogues of classical monophosphine complexes (Scheme 3). The gold chloride adduct of **1**, $\mathbf{1_{Au}}$, is readily accessed by the reaction of **1** with one equivalent of ClAu·SMe_2. The room temperature NMR spectra of $\mathbf{1_{Au}}$ in $CDCl_3$ are broad, similarly to those of $\mathbf{1_S}$ and $\mathbf{1_{Se}}$, and indicate restricted rotation about the P–C bond. DFT analysis with implicit solvation model for $CDCl_3$ showed that the rotation of the CAAC moiety about the P–C bond has a barrier of 13.83 kcal mol^{-1}, in agreement with experimental observations. The solid-state structure of $\mathbf{1_{Au}}$ (Fig. 5, top left) resembles more $\mathbf{1_{Cs}}$ than $\mathbf{1_{C1}}$ and shows close association of the gold center with the phenyl ring of the diisopropylphenyl moiety (distance from Au to ring centroid is 3.333 Å), consistent with a gold···arene interaction that is a hallmark of many effective gold catalysts.[62,63] The steric profile of **1** was evaluated by calculation of the topographic steric map and percent buried volume using the SambVca 2.1 tool developed by Cavallo and coworkers (Fig. 5, bottom).[64] Compound **1** provides considerable steric bulk ($\%V_{bur}$ = 47.7%), comparable to Buchwald-type biaryl phosphine ligands (*cf.* $\%V_{bur}$ of 46.7% and 50.9% for CyJohnPhos and JohnPhos),[65] with a highly asymmetric steric profile due to the presence of the aforementioned gold···arene interaction.

Having established the steric properties of **1**, we sought to evaluate the donor ability by synthesis of an appropriate metal carbonyl complex.[66] Unfortunately, attempts to coordinate **1** to rhodium(I) precursor $[(CO)_2RhCl]_2$ led to degradation of **1** and no apparent formation of any rhodium phosphine complexes, as indicated by the lack of AX_2 or AXY spin systems or readily apparent coupling to rhodium in the $^{31}P\{^1H\}$ NMR spectra of the reaction mixtures. Owing to toxicity concerns with $Ni(CO)_4$, the donor ability of **1** was evaluated *in silico* using DFT by calculation of the IR spectra of the putative nickel tricarbonyl complex with **1**, denoted $\mathbf{1_{Ni}}$, and comparing the result to data for known tricarbonyl complexes investigated at the same level of theory (Fig. S13†).[67] This methodology indicates that **1** has a computed Tolman electronic parameter (cTEP) of 2070 cm^{-1}, which is comparable to triaryl phosphines lacking donor substituents, suggestive of modest donor ability. Exploiting the flexibility afforded by computational protocols, the effect of the phosphazene chloride substituents on donor ability was also investigated by replacing them with modestly donating methyl substituents (Fig. S14†). This modification had significant influence on the cTEP value, with a red-shift of 21 cm^{-1} to 2049 cm^{-1}, suggesting that the framework of **1** may have utility as an electronically modular ligand platform.

Lastly, as phosphines are known to effectively bind the Cp*RuCl fragment[68,69] to give synthetically useful compounds with metal to ligand stoichiometry depending on the bulk of the ligand, the reactivity of **1** with $[Cp^*RuCl]_4$ (ref. 70) was explored. Compound **1** was found to react with 0.25 eq. $[Cp^*RuCl]_4$ in THF with immediate formation of a dark purple solution (Scheme 3).The room temperature $^{31}P\{^1H\}$ NMR spectrum of **1** in C_6D_6 indicated the presence of a single AMX spin system, consistent with the formation of an asymmetric 1 : 1 adduct of **1** with Cp*RuCl, $\mathbf{1_{Ru}}$. The composition of $\mathbf{1_{Ru}}$ was further supported by

© 2025 The Author(s). Published by the Royal Society of Chemistry

Open Access Article. Published on 24 April 2025. Downloaded on 2/22/2026 5:57:45 PM. This article is licensed under a Creative Commons Attribution-NonCommercial 3.0 Unported Licence.

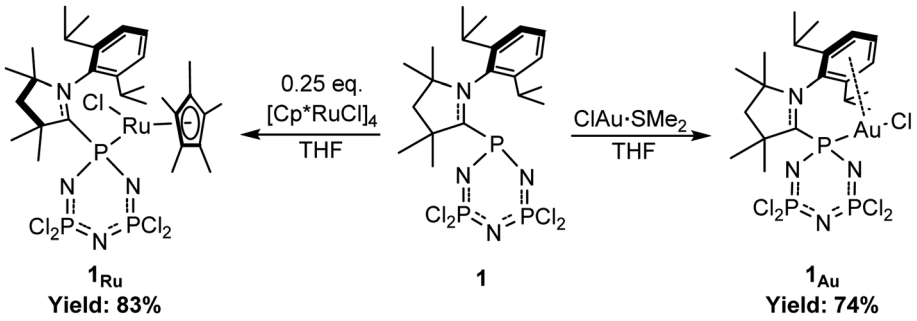

Scheme 3 Metalation reactions of **1**.

determination of its solid-state structure by single crystal X-ray diffraction studies, indicating that the chloride ligand at ruthenium orients itself above the $CAAC^{Me}$ moiety with a C···Cl distance of 3.554(2) Å, that is, only slightly longer than the sum of van der Waals radii for the respective elements. Given the acceptor nature of the $CAAC^{Me}$ fragment in $\mathbf{1_S}$ and $\mathbf{1_{Se}}$, the possibility of a weak halogen···π interaction was raised. However, computational analyses gave no support for such phenomenon, suggesting that the preferred ligand orientation in $\mathbf{1_{Ru}}$ more likely results from a combination of electrostatic H···Cl interactions as well as steric factors.

The UV-Vis spectrum of $\mathbf{1_{Ru}}$ in THF (Fig. S15†) features a broad asymmetric absorption band at 492 nm ($\varepsilon_{492} = 4.67 \times 10^3$ M^{-1} cm^{-1}), with a visible shoulder at *ca.* 570 nm. This is atypical for analogous complexes featuring classical phosphines that often show relatively weak d → d transitions at wavelengths greater than 550 nm.[69] Accordingly, TD-DFT calculations with implicit THF solvation were performed for $\mathbf{1_{Ru}}$, illustrating that the strongest absorption in the visible region arises from the $S^0 \rightarrow S^4$ transition at 470 nm, in good agreement with the experiment. Calculation of the natural transition orbitals (NTOs)[71] for this excitation are suggestive of

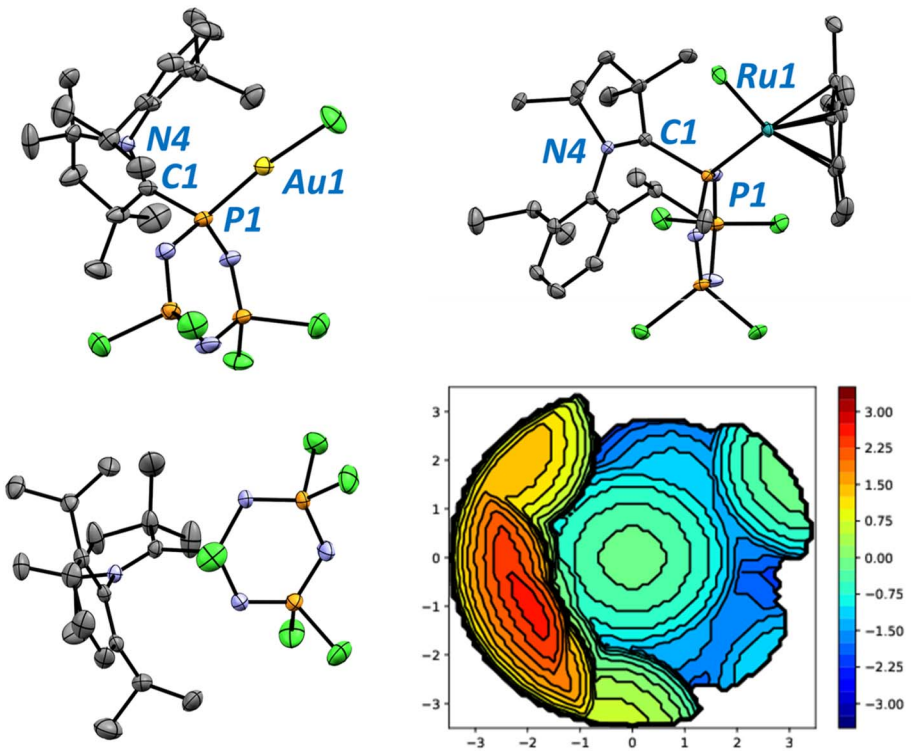

Fig. 5 Molecular structures of $\mathbf{1_{Au}}$ (top, left) and $\mathbf{1_{Ru}}$ (top, right), and topographic steric map for calculation of $\%V_{bur}$ of $\mathbf{1_{Au}}$ using the shown orientation (bottom). Ellipsoids are drawn at 50% probability. Hydrogen atoms are omitted for clarity. Select bond lengths (Å) and angles (°) for $\mathbf{1_{Au}}$ [calculated values in square brackets]: Au1–P1 2.2184(6) [2.223]; Au1–Cl1 2.2874(8) [2.284]; P1–C1 1.888(2) [1.878]; C1–N4 1.287(3) [1.291]; P1–N1 1.633(2) [1.628]; N1–P2 1.554(2) [1.561]; P2–N2 1.586(2) [1.589]; C1–P1–Au1 117.62(7) [114.7]; C1–P1–N1 102.73(9) [103.7]; N1–P1–N3 111.8(1) [111.7]. Select bond lengths (Å) and angles (°) for $\mathbf{1_{Ru}}$ [calculated values in square brackets]: Ru1–P1 2.3283(5) [2.315]; Ru1–Cl1 2.3805(6) [2.359]; P1–C1 1.866(2) [1.850] C1–N4 1.312(2) [1.307]; P1–N1 1.633(2) [1.651]; N1–P2 1.552(1) [1.557]; P2–N2 1.588(2) [1.587]; C1–P1–Ru1 104.45(5) [104.1]; C1–P1–N1 101.96(7) [102.4]; N1–P1–N3 110.08(7) [111.0]; P1–Ru1–Cl1 106.51(2) [106.9]; Ru1–P1–N1 116.42(5) [115.7].

Open Access Article. Published on 24 April 2025. Downloaded on 2/22/2026 5:57:45 PM. This article is licensed under a Creative Commons Attribution-NonCommercial 3.0 Unported Licence.

a metal-to-ligand charge-transfer (MLCT), with the electron NTO having clear ruthenium d-orbital character, while the hole NTO is predominantly the C–N π*-orbital at the CAAC moiety (Fig. 6); similar features are seen in the associated electron density difference plot. Further evidence for the assignment is provided by calculation of its D_{CT} index that quantifies the distance of charge-transfer as the distance between barycenters of electron depletion and augmentation of a given transition.[72,73] For the $S^0 \rightarrow S^4$ transition, a D_{CT} index of 2.545 Å was obtained, consistent with charge-transfer, serving to highlight the photophysical non-innocence of **1** as a ligand, which is unusual for monodentate phosphines.

Reduction of 1

Having explored the oxidation and metalation chemistry of **1**, the ability of CAAC^{Me} to mediate multi-site reduction of hexachlorophosphazene was explored. Treating **1** with comparatively mild metal-based reductants zinc and manganese in the presence of one or two additional equivalents of CAAC^{Me} gave an intractable mixture of products, while the use of a stronger reductant magnesium led to complete loss of all resonances in the $^{31}P\{^1H\}$ NMR spectrum. In contrast, treatment of **1** with two equivalents of stoichiometric strong reductants, such as KC_8 or alkali metal naphthalenides, in the presence of excess CAAC^{Me} led to partial consumption of **1**, as assayed by $^{31}P\{^1H\}$ NMR spectrometry that showed the formation of a new A_2X spin system with δ_P = 105.8 (A) and −4.3 (X) ppm, that is, only slightly shifted from those of **1** (δ_P = 104.3 and 4.6 ppm), suggestive of partial reduction of **1** to give a new species **2**. Treatment of the reaction mixture with additional reductant and CAAC^{Me} did not lead to full conversion of **1** to **2** but to complete loss of signals in the $^{31}P\{^1H\}$ NMR spectrum, which, combined with the incomplete conversion when using appropriate stoichiometry, may be indicative of kinetically competitive over-reduction to an unidentified species.

As silylated pyrazines have previously been demonstrated to effect the controlled reduction of phosphazenes,[26] 1,4-bis(trimethylsilyl)-dihydropyrazine (TMS-DHP, also called Mashima's reagent)[74,75] was explored as a potential reductant for the selective generation of hemi-reduced species **2** (Scheme 4). Treatment of **1** with one equivalent of TMS-DHP and two equivalents of CAAC^{Me} in THF gave smooth conversion to **2**,

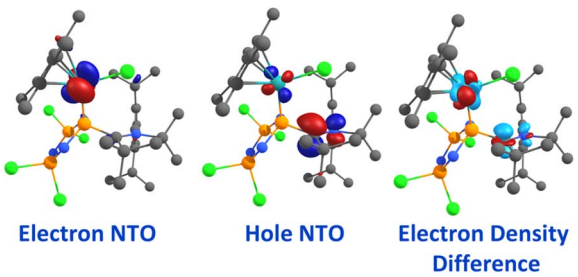

Fig. 6 Natural transition orbitals (NTOs, isovalue = ±0.08 a.u.) and the electron density difference map (isovalue = ±0.008 a.u.; red = depletion, teal = accumulation) for the $S^0 \rightarrow S^4$ transition of $\mathbf{1}_{Ru}$.

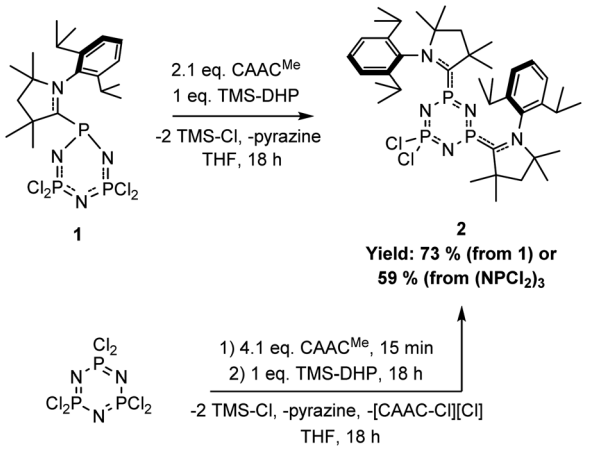

Scheme 4 Reduction of **1** to **2** using 1,4-bis(trimethylsilyl)-dihydropyrazine (TMS-DHP) in the presence of excess CAAC^{Me} and the direct synthesis of **2** from hexachlorophosphazene with TMS-DHP and CAAC^{Me}.

which could be isolated as a navy blue microcrystalline solid in good yield. Conveniently, **2** could also be prepared directly from hexachlorophosphazene without isolation of **1** in comparable yields (Scheme 4). The room temperature ^1H NMR spectrum of **2** in C_6D_6 possesses only a single set of resonances for the CAAC^{Me} substituents, which suggests symmetric orientation of pyrrolidine rings or a fast dynamic process by which the faces of the rings interconvert (*vide infra*). Attempts to extend the synthetic methodology by either reducing **1** in the presence of an NHC, 1,3-bis(2,6-diisopropylphenyl)imidazol-2-ylidene,[76] or by reducing **A** with CAAC^{Me} and external reductants were met with failure.

The solid-state structure of **2**, as determined by single crystal X-ray diffraction experiments, revealed an asymmetric structure with the two CAAC^{Me} moieties *trans*-oriented with respect to the phosphazene ring and with different relative orientation of their

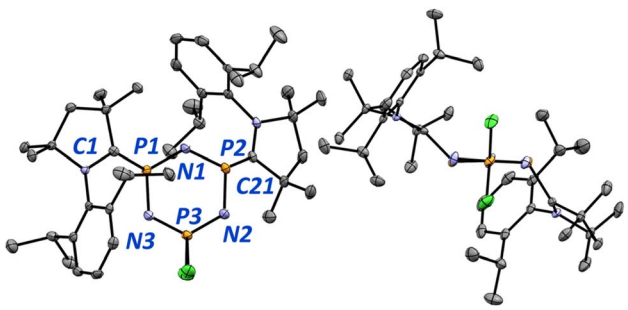

Fig. 7 Molecular structure of **2** shown from two perspectives. Ellipsoids are drawn at 50% probability. Hydrogen atoms are omitted for clarity. Select bond lengths (Å) and angles (°) for **2** [calculated values in square brackets]: P1–C1 1.752(2) [1.736]; P2–C21 1.825(2) [1.772]; C1–N4 1.356(3) [1.346]; C21–N5 1.328(3) [1.336]; P1–N1 1.610(2) [1.617]; N1–P2 1.624(2) [1.615]; P2–N2 1.658(2) [1.644]; N2–P3 1.560(2) [1.568]; C1–P1–N1 112.3(1) [114.1]; C21–P2–N1 112.2(1) [115.5]; P1–N1–P2 124.8(1) [122.1]; N1–P1–N3 116.4(1) [116.4]; C1–P1–N3 110.9(1) [112.0].

© 2025 The Author(s). Published by the Royal Society of Chemistry

Open Access Article. Published on 24 April 2025. Downloaded on 2/22/2026 5:57:45 PM. This article is licensed under a Creative Commons Attribution-NonCommercial 3.0 Unported Licence.

diisopropylphenyl rings (Fig. 7). Unlike in **1**, the phosphazene ring is effectively planar and possesses notably short bonds between the reduced phosphorus centers and the nitrogen atom between them, P1–N1 = 1.610(2) Å and P2–N1 = 1.624(2) Å, which are shorter than those in **1** and suggest partial multiple bond character.[77,78] Saliently, the reduced phosphorus centers exhibit highly inequivalent P–C bond lengths of 1.752(2) Å and 1.825(2) Å. While this feature is reproduced by DFT optimization of the structure, the difference in calculated bond lengths is much smaller, only 0.04 Å, suggesting that the experimentally observed disparity is not only due to the steric strain caused by the orientation of the diisopropylphenyl rings but also because of crystallographic packing effects.

Given the planar arrangement of the phosphazene ring in **2**, its unusual coloration, and its NMR spectra, which are incongruent with its solid-state structure, further computational analyses were performed. Despite the CAAC^{Me} fragments not being co-planar with the phosphazene ring, the Kohn–Sham HOMO and LUMO of **2** represent those of a seven-membered π-system comprising the carbon and nitrogen atoms of both CAAC^{Me} substituents, the reduced phosphorus centers, and the nitrogen atom connecting them (Fig. 8). This electronic structure rationalizes the intense coloration of **2**, whose UV-Vis absorption spectrum in toluene (Fig. S16†) is characterized by the presence of a strong absorption centered at 561 nm ($\varepsilon_{561} = 1.29 \times 10^4\ M^{-1}\ cm^{-1}$), as is typical for a π → π* transition. This assertion is further supported by TD-DFT calculations with implicit solvation for toluene, which show a high-intensity band at 536 nm with HOMO → LUMO character.

Further experimental work was performed to rationalize the spectroscopic data for **2**. First, low-temperature NMR studies were performed at 198 K in toluene-d_8, revealing an exceptionally broad ^{1}H NMR spectrum, while the $^{31}P\{^1H\}$ NMR spectrum shows decoalescence of the resonances attributed to the reduced phosphorus centers (Fig. S17 and S18†), with the resonance for the PCl_2 moiety remaining sharp. These results indicate that the faces of the pyrrolidine rings interconvert at higher temperatures, the chemically most reasonable process for it being inversion about phosphorus. The plausibility of such process was probed with DFT calculations employing implicit solvation for toluene that identified a second isomer for **2** in which the two CAAC^{Me} moieties are *cis*-oriented with respect to the phosphazene ring (Fig. S19†). Because the two diisopropylphenyl rings have nearly identical relative orientation, this isomer has overall pseudo-C_s symmetry, $\mathbf{2}_{Cs}$, and Gibbs free energy that is only 3.25 kcal mol^{-1} higher than the asymmetric global minimum, denoted hereafter $\mathbf{2}_{C1}$. While phosphorus does not normally invert, the presence of strongly π-accepting substituents, such as CAAC, can significantly lower the energy of planar intermediates or transition states.[79] In good agreement with the above, the Gibbs free energy of activation for inversion about phosphorus was calculated to be only 5.04 kcal mol^{-1} for $\mathbf{2}_{Cs}$.

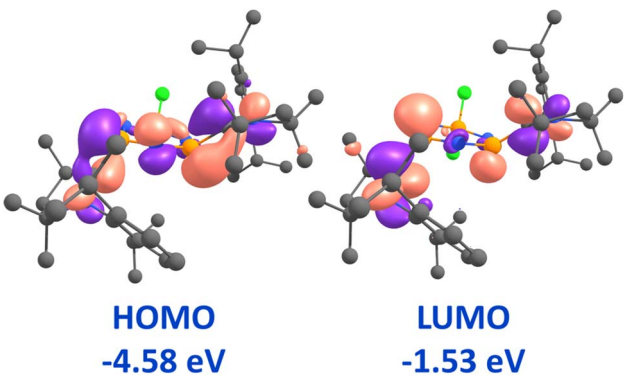

Fig. 8 Frontier Kohn–Sham orbitals of **2** (isovalue ±0.04 a.u.).

The reactivity of **2** was examined first by attempting to effect reduction of the final PCl_2 moiety. Unfortunately, all attempts using a wide variety of reducing agents (Li, Na, K, Na/K, potassium naphthalenide, KC_8, Mg, Mn, KFp, $LiHBEt_3$, or $Na_2Fe(CO)_4$) under various conditions, in the presence or absence of additional equivalent(s) of CAAC^{Me}, led to degradation of **2**, consistent with observations made during its attempted synthesis. Therefore, other potential reactivity was explored. As the lone pairs on phosphorus in **2** are engaged in conjugation, their chemical availability is questionable; thus, attempts to illicit oxidative chemistry analogous to that of **1** was explored (Scheme 5). Treatment of **2** with an excess of selenium resulted in rapid color change from blue to orange. Room temperature $^{31}P\{^1H\}$ NMR spectrometry in $CDCl_3$ indicated complete consumption of **2** and formation of a new A_2X spin system with $\delta_P = 16.3$ (A) and 4.2 (X) ppm, the former resonance possessing distinct ^{77}Se satellites that appear as multiplets. This may be due to second order coupling owing to magnetic inequivalence in the $^{77}Se^{XX}Se$ isotopologues, resulting in an ABMX spin system. The ^{77}Se NMR spectrum of the product consists of a doublet of broad resonances centered at $\delta_{Se} = 230.5$ ppm with a $^1J_{P-Se}$ coupling constant of 648 Hz. Subsequent structural analysis by single crystal X-ray diffraction confirmed the product to be the doubly oxidized $\mathbf{2}_{Se}$ (Fig. 9). Both the ^{1}H NMR data and the solid-state structure of $\mathbf{2}_{Se}$ are consistent with C_2 molecular symmetry, indicating that the CAAC^{Me} moieties are locked in the same rotational orientation. The C···Se distance in $\mathbf{2}_{Se}$ is slightly shorter than in $\mathbf{1}_{Se}$, 2.911(2) Å, indicative of a sizable through-space interaction. The UV-Vis spectrum of $\mathbf{2}_{Se}$ in THF is analogous to that of $\mathbf{1}_{Se}$, with an identical λ_{max} = 387 nm and an extinction coefficient approximately double that of $\mathbf{1}_{Se}$ ($\varepsilon_{387} = 1.15 \times 10^4\ M^{-1}\ cm^{-1}$), congruous with the presence of two chromophores per molecule of $\mathbf{2}_{Se}$.

With the above reaction demonstrating the availability of the phosphorus lone pairs of **2** to participate in chemical reactions, the ability of **2** to serve as a ligand in transition metal chemistry was explored. Treatment with two equivalents of $ClAu{\cdot}SMe_2$ results in the rapid formation of a gold mirror and degradation of **2** to a brown intractable material; accordingly, **2** is also degraded by mild one electron oxidants such as trityl cation and ferrocenium, consistent with its extreme electron richness. In contrast, treatment of **2** with a half an equivalent of $[Cp^*RuCl]_4$ results in conversion to a new product **3**, characterized by an AMX spin system in the $^{31}P\{^1H\}$ NMR spectrum of the reaction mixture. While an AMX spin system could be indicative of

Open Access Article. Published on 24 April 2025. Downloaded on 2/22/2026 5:57:45 PM. This article is licensed under a Creative Commons Attribution-NonCommercial 3.0 Unported Licence.

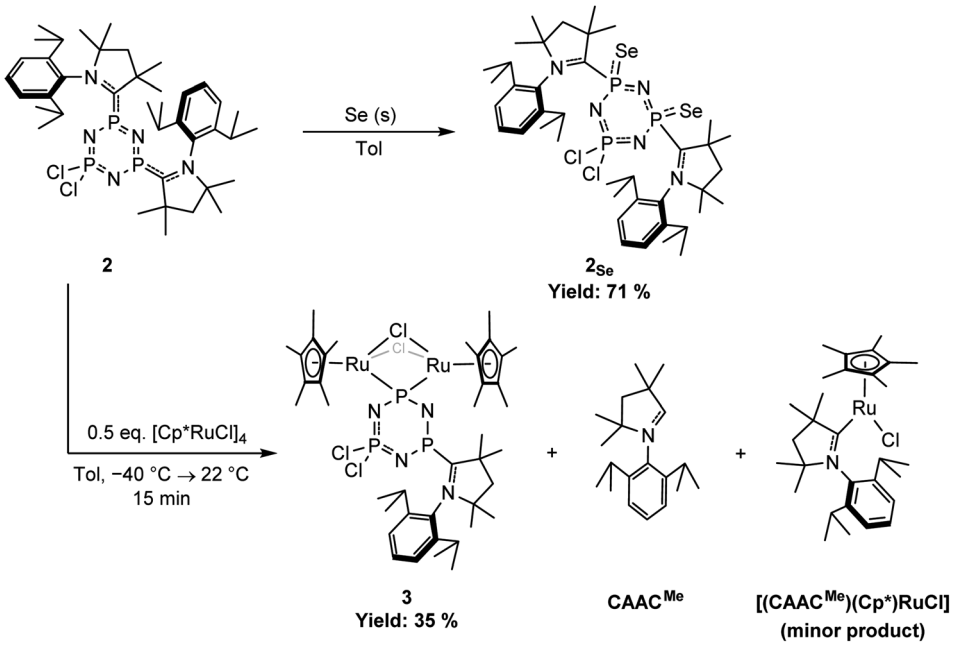

Scheme 5 Reactivity of **2** towards selenium and $[Cp^*RuCl]_4$.

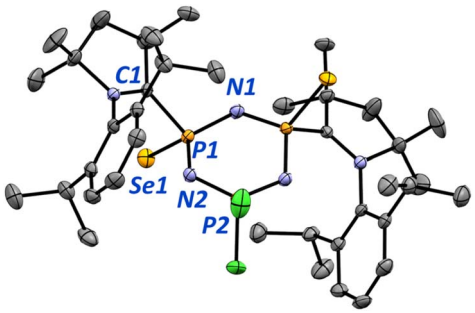

Fig. 9 Molecular structure of $\mathbf{2_{Se}}$. Ellipsoids are drawn at 50% probability. Hydrogen atoms are omitted for clarity. Select bond lengths (Å) and angles (°) for $\mathbf{2_{Se}}$: P1–Se1 2.1212(8) [2.120]; P1–C1 1.845(2) [1.833]; C1–N4 1.305(3) [1.307]; P1–N1 1.601 [1.596]; P1–N2 1.620(2) [1.614]; P2–N2 1.565 [1.567]; C1–P1–Se1 94.18(7) [93.1]; C1–P1–N1 106.3 [106.7]; P1–N1–P1′ 124.0 [124.7]; N1–P1–N2 114.6 [114.6].

formation of a ruthenium phosphine complex akin to $\mathbf{1_{Ru}}$, the dramatic downfield chemical shift of one of the resonances (δ_P = 254.1, 108.2, and 1.5 ppm) is inconsistent with this formulation (*cf.* δ_P = 99.1 ppm for $\mathbf{1_{Ru}}$). Further, the ^{1}H NMR spectrum of **3** is indicative of at least two Cp* containing compounds and three CAAC containing species, two major and one minor. One of the major products could be identified as free $CAAC^{Me}$, while the minor product was identified as $[(CAAC^{Me})(Cp^*)RuCl]$, by comparison of known NMR spectra and independent synthesis (Fig. S20†), respectively.

The formulation and structure of **3** was determined by fractional crystallization from the reaction mixture and subsequent X-ray diffraction studies. As implied by the spectroscopic data, **3** arises from the formal loss of $CAAC^{Me}$ from **2**, followed by geminal dimetallation of the phosphorus center by a $[Cp^*RuCl]_2$ fragment to yield a spirocyclic bimetallic complex bridged by two chlorides and the endocyclic phosphorus center (Fig. 10). This unusual reaction is, to our knowledge, the first formal electrophilic displacement of a carbene. While the mechanism of the reaction was not probed with experiments, we note that **2** is stable for at least two weeks in C_6D_6 solution at room temperature and overnight at 353 K, and is unlikely to spontaneously release $CAAC^{Me}$. In agreement with this result, DFT calculations probing the dissociation of $CAAC^{Me}$ from **2** resulted in a highly endergonic Gibbs free energy change of 21.57 kcal mol^{-1}, indicating that the associated transition state,

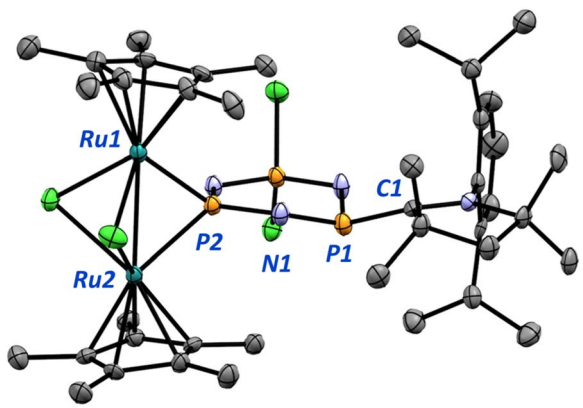

Fig. 10 Molecular structure of **3**. Ellipsoids are drawn at 50% probability. Hydrogen atoms are omitted for clarity. Select bond lengths (Å) and angles (°) [calculated values in square brackets]: P1–C1 1.761(4) [1.722]; C1–N4 1.345(6) [1.344]; P1–N1 1.634(4) [1.609]; N1–P2 1.609(4) [1.603]; P2–Ru1 2.328(1) [2.312]; Ru1–Ru2 2.7339(6) [2.724]; Ru1–Cl3 2.4560(9) [2.498]; Ru1–P1–Ru2 71.89(3) [72.0]; Ru1–Cl3–Ru2 66.87(3) [65.9].

© 2025 The Author(s). Published by the Royal Society of Chemistry

Open Access Article. Published on 24 April 2025. Downloaded on 2/22/2026 5:57:45 PM. This article is licensed under a Creative Commons Attribution-NonCommercial 3.0 Unported Licence.

if any, would be even higher in energy. Therefore, one may postulate that the loss of $CAAC^{Me}$ is induced by the introduction of $[Cp^*RuCl]_4$. A reasonable mechanistic proposal involves the dissociation of $[Cp^*RuCl]_4$ in solution to two units of $[Cp^*RuCl]_2$, as this process has a calculated Gibbs free energy change of only 13.88 kcal mol^{-1} in the gas phase. Subsequent association of the ruthenium centers in $[Cp^*RuCl]_2$ with the lone pairs on phosphorus and nitrogen in **2** would weaken the π-component of the C–P bond, leading to release of $CAAC^{Me}$ and subsequent formation of **3** upon rearrangement of the bound $[Cp^*RuCl]_2$ fragment. Overall, the calculated Gibbs free energy change for the process **2** + 0.5 $[Cp^*RuCl]_4$ → **3** + $CAAC^{Me}$ is slightly exergonic, −3.61 kcal mol^{-1}. A full computational study of the mechanism of this process is beyond the scope of this work.

Thermal properties of 1 and 2

Having explored the small molecule chemistry of **1** and **2**, and given the known utility of phosphazenes containing endocyclic heteroatoms as precursors to main-chain substituted poly-phosphazenes accessible by thermal ring opening polymerization (ROP),[80–82] the thermal properties of **1** and **2** were explored by differential scanning calorimetry (DSC) to determine their viability as polymer precursors. The differential thermogram of **1** reveals a single exothermic event at 161 °C (onset, peak = 168 °C), which is not observed in subsequent heating cycles (Fig. S21†), indicative of either decomposition or thermal ROP without melting; in contrast, the differential thermogram of **2** features an irregular exothermic peak at 137 °C (onset, peak = 151 °C), followed by several others at higher temperatures, strongly suggestive of decomposition (Fig. S22†). Accordingly, heating **1** or **2** to near the exotherm onset temperature (165 °C and 140 °C, respectively) in a flame sealed Pyrex tube under vacuum resulted in the formation of a glassy red-orange solid and a black tar, respectively. While the latter is consistent with decomposition and was not further examined, the former may be indicative of the desired reactivity and attempts to analyze the material were made. Unfortunately, the material accessed by thermal treatment of **1** was completely insoluble in all common solvents and highly sensitive, fuming in air, which precluded further investigation. Hypothesizing that the intractability of this material may be due to its uncontrolled synthesis, an alternative route to the desired polymer was sought.

Synthesis and reactivity of poly-1

As the reductive protocol to access **1** is exceptionally mild, the ability of $CAAC^{Me}$ to effect the direct reduction of poly-chlorophosphazene was examined. End-capped linear poly-chlorophosphazene was synthesized by the living cationic polymerization of *P*,*P*,*P*-trichloro-*N*-trimethylsilyl-phosphoranimine[83,84] by modification of literature procedures[85,86] and immediately reacted with 2.2 eq. of $CAAC^{Me}$ upon synthesis (Scheme 6). This resulted in immediate formation of a precipitate and a color change to bright orange, akin to the synthesis of **1**. Following filtration to remove the precipitate, a bright yellow solid could be isolated from the reaction mixture by dropwise addition to *n*-hexane. Analysis of the material by $^{31}P\{^1H\}$ NMR spectrometry revealed absence of poly-chlorophosphazene and the presence of two broad resonances in a 1 : 2 ratio at $\delta_P = 77.1$ and −31.6 ppm, that are shifted upfield to that of **1**, which is consistently observed when comparing the chemical shift of phosphazene polymers to their (formal) cyclic monomers.[80–82] This spectral data is suggestive of the regiospecific, direct reduction of poly-chlorophosphazene to the desired product poly-**1**. The regiospecificity and stoichiometry of the reduction can be readily explained on the basis of reduction potentials, whereby the reduction and ligation of one phosphorus center renders the two proximal PCl_2 units along the main chain too electron rich for CAAC to effect their reduction; accordingly, addition of further $CAAC^{Me}$ was not observed to bring about additional reduction events. Likewise, the ^1H NMR spectrum of poly-**1** features broad resonances attributable to embedding a CAAC fragment into a polymer backbone; however, CAAC derived small molecule impurities are also noted, which may arise due to free $CAAC^{Me}$ and/or $[CAAC^{Me}–Cl][Cl]$ becoming entrained in the polymer, and could unfortunately not be removed by reprecipitation of the polymer.

The UV-Vis spectrum of poly-**1** is in good agreement with that observed for **1**, with a $\lambda_{max} = 437$ nm (*cf.* 438 nm for **1**), suggesting that the chromophore of **1**, that is, the P-$CAAC^{Me}$ fragment, is present in poly-**1**; however, the extinction coefficient is reduced by an order of magnitude ($\varepsilon_{437} = 3.5 \times 10^2$ M^{-1} cm^{-1}), which can be explained by the different rotational orientations of the $CAAC^{Me}$ moieties adopted by the flexible open chain poly-**1**, compared to **1**. Examination of the DSC thermogram of poly-**1** reveals a nearly identical exothermic event to **1** (onset = 161 °C) that is lost in subsequent heating cycles (Fig. S23†). Heating poly-**1** to this temperature leads to formation of a red-brown glassy insoluble solid, as occurs when heating **1**. While assigning the exact chemical events that occur are fraught, the crosslinking of poly-phosphazenes at or near the ROP

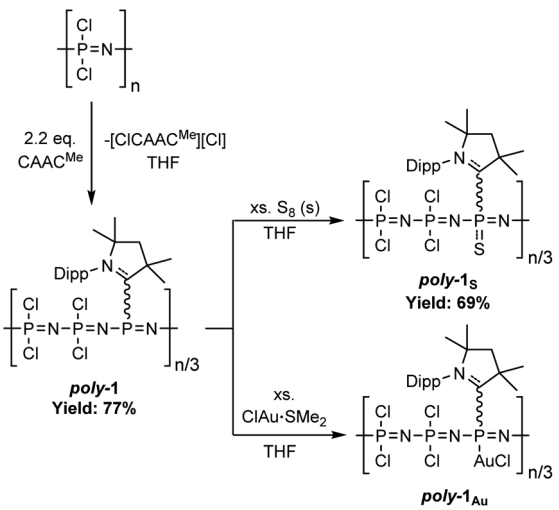

Scheme 6 Reduction of poly-chlorophosphazene to poly-**1** and its subsequent reactivity with excess S_8 and $ClAu·SMe_2$. Dipp = 2,6-diisopropylphenyl.

Open Access Article. Published on 24 April 2025. Downloaded on 2/22/2026 5:57:45 PM. This article is licensed under a Creative Commons Attribution-NonCommercial 3.0 Unported Licence.

temperature is a common issue[11,80,81] and would be consistent with the observed macroscopic outcomes, which in turn strongly suggest that ROP of **1** is not a viable route to poly-**1**.

With poly-**1** in hand, the viability of transposing the reactivity of **1** to the polymeric system to enable further derivatization was explored. Firstly, attempts to further reduce poly-**1** were unsuccessful, as treatment with TMS-DHP in the presence of $CAAC^{Me}$ led to an intractable mixture of products. In contrast, the oxidation of poly-**1** with an excess of sulfur proceeds smoothly and rapidly, with quantitative conversion achieved within 5 minutes to yield poly-$\mathbf{1_S}$. The $^{31}P\{^1H\}$ NMR spectrum of poly-$\mathbf{1_S}$ is consistent with oxidation at the phosphorus(III), as evidenced by the large upfield shift of the resonance to δ_P = 10.4 ppm, as was observed in the oxidation of **1** to $\mathbf{1_S}$. The UV-Vis spectrum of poly-$\mathbf{1_S}$ matches that of $\mathbf{1_S}$, with a λ_{max} = 341 nm, though with a reduced extinction coefficient ($\varepsilon_{341} = 1.49 \times 10^2\ M^{-1}\ cm^{-1}$). The magnitude of the reduction, in comparison to the difference between the extinction coefficients of **1** and poly-**1**, is smaller, which may be caused by a more rigid structure facilitated by intramolecular through-space C···S interactions. The lone pairs in poly-**1** are also chemically available for metalation reactions, as evidenced by reaction with $ClAu\cdot SMe_2$ that quantitatively converts poly-**1** to a new species poly-$\mathbf{1_{Au}}$, as determined by $^{31}P\{^1H\}$ NMR spectrometry. Unfortunately, poly-$\mathbf{1_{Au}}$ is highly light sensitive, readily depositing a gold mirror, which hinders its isolation and complete characterization. Despite this, the formation of poly-$\mathbf{1_{Au}}$ provides evidence that poly-**1** may be utilized as platform for the synthesis of metallopolymers that could be used as heterogenous catalysts or ceramic precursors.

Conclusions

In summary, this work presents the cyclic (alkyl)(amino)carbene mediated single-site and unprecedented multi-site reduction of hexachlorophosphazene, as well as a thorough experimental and computational study of the reactivity, structure, and bonding of the reduced species. The single-site reduced **1** exhibits oxidation and metalation chemistry typical of phosphines, however, the CAAC-centered LUMO bestows the resultant compounds with unusual properties, capable of engaging in acceptor-type (Z-type) secondary coordination sphere interactions, as well as serving as an acceptor orbital in photophysical transitions. Further, **1** may engage in more classical metal···arene secondary coordination donor-type interactions, possesses an encumbering steric profile, and should be electronically tunable by distal modification of the phosphazene ring, all promising traits for the use of **1** and its derivatives in transition metal catalysis. Further reduction of **1** in the presence of $CAAC^{Me}$ results in the formation of **2**, which features a non-planar π-system spanning the two $CAAC^{Me}$ moieties and the reduced PNP fragment, that underscores the ability of reduced phosphazenes to engage in conjugation. Treatment of **2** with $[Cp^*RuCl]_4$ results in the formation of a spirocyclic bimetallic complex **3** arising from the unusual electrophilic displacement of a stable carbene. Importantly, the reductive methodology utilized in the synthesis of **1** can be readily applied to the regiospecific controlled reduction of poly-chlorophosphazene to poly-**1**, which represents a new class of inorganic polymers. The lone pair of the reduced phosphorus center in poly-**1** is chemically available, as demonstrated by successful chemical oxidation and metalation in direct analogy to the chemistry of **1**, which underscores the utility of this ring system to serve as an effective model for the chemistry of poly-**1**. Optimization of the synthesis of poly-**1**, as well as further studies of its properties and chemistry are currently underway.

Data availability

The data supporting this article have been included as part of the ESI.† Experimental and characterization details for all new compounds, including spectroscopic data, ESI figures,† and full computational details (PDF). Coordinates for all optimized structures are available as a separate file (XYZ). Crystallographic data for complexes **1**, $\mathbf{1_S}$, $\mathbf{1_{Se}}$, $\mathbf{1_{Au}}$, $\mathbf{1_{Ru}}$, **2**, $\mathbf{2_{Se}}$, **3**, and [**(CAAC)(Cp*)RuCl**] are provided as a CIF file, or can be obtained free of charge from **https://www.ccdc.cam.ac.uk/structures/** CCDC: 2383407–2383415 (CIF).

Author contributions

E. L. designed and carried out the synthetic work. B. P. acquired and processed the SC-XRD data, E. L. carried out the structure refinement. DFT studies were performed by R. S., E. L. and H. T. Supervision was shared between E. L., I. M. and H. T. The manuscript was drafted by E. L. and revised by E. L. and H. T., and approved by all authors.

Conflicts of interest

The authors declare no competing financial interests.

Acknowledgements

I. M. thanks the Canadian Government for a Canada 150 Research Chair, NSERC for a Discovery Grant, and the University of Victoria for start-up funds. E. L. thanks NSERC for a Postdoctoral Fellowship. H. M. T. and R. S. thank the University of Jyväskylä for funding. Digital Research Alliance of Canada and the Finnish Grid and Cloud Infrastructure (persistent identifier urn:nbn:fi:research-infras-2016072533) are acknowledged for access to computing resources.

References

1 J. von Liebig, *Ann. Pharm.*, 1834, 11–12.
2 D. P. Craig and N. L. Paddock, *Nature*, 1958, **181**, 1052–1053.
3 A. E. Reed and P. V. Schleyer, *J. Am. Chem. Soc.*, 1990, **112**, 1434–1445.
4 A. B. Chaplin, J. A. Harrison and P. J. Dyson, *Inorg. Chem.*, 2005, **44**, 8407–8417.
5 H. Sun, *J. Am. Chem. Soc.*, 1997, **119**, 3611–3618.
6 H. Stokes, *Am. Chem. J.*, 1895, **17**, 275–291.
7 H. Stokes, *Am. Chem. J.*, 1896, **18**, 629–663.

© 2025 The Author(s). Published by the Royal Society of Chemistry

Open Access Article. Published on 24 April 2025. Downloaded on 2/22/2026 5:57:45 PM. This article is licensed under a Creative Commons Attribution-NonCommercial 3.0 Unported Licence.

8 H. Stokes, *Am. Chem. J.*, 1897, **19**, 782–796.
9 H. R. Allcock, R. L. Kugel and K. J. Valan, *Inorg. Chem.*, 2002, **5**, 1709–1715.
10 H. R. Allcock and R. L. Kugel, *J. Am. Chem. Soc.*, 2002, **87**, 4216–4217.
11 S. Rothemund and I. Teasdale, *Chem. Soc. Rev.*, 2016, **45**, 5200–5215.
12 K. S. Ogueri, K. S. Ogueri, H. R. Allcock and C. T. Laurencin, *J. Vac. Sci. Technol., B: Nanotechnol. Microelectron.:Mater., Process., Meas., Phenom.*, 2020, **38**, 030801.
13 X. Zhou, S. L. Qiu, X. W. Mu, M. T. Zhou, W. Cai, L. Song, W. Y. Xing and Y. Hu, *Composites, Part B*, 2020, **202**, 108397.
14 H. R. Allcock and N. L. Morozowich, *Polym. Chem.*, 2012, **3**, 578–590.
15 H. R. Allcock, *Polymer*, 2022, **249**, 124761.
16 H. R. Allcock, *Chem. Rev.*, 1972, **72**, 315.
17 H. R. Allcock and C. Chen, *J. Org. Chem.*, 2020, **85**, 14286–14297.
18 C. W. Allen, *Chem. Rev.*, 2002, **91**, 119–135.
19 A. M. Caminade, *Chem. Soc. Rev.*, 2016, **45**, 5174–5186.
20 H. Henke, O. Bruggemann and I. Teasdale, *Macromol. Rapid Commun.*, 2017, **38**, 1600644.
21 S. M. Al-Rafia, M. J. Ferguson and E. Rivard, *Inorg. Chem.*, 2011, **50**, 10543–10545.
22 H. R. Allcock, L. J. Wagner and M. L. Levin, *J. Am. Chem. Soc.*, 2002, **105**, 1321–1327.
23 P. P. Greigger and H. R. Allcock, *J. Am. Chem. Soc.*, 2002, **101**, 2492–2493.
24 P. R. Suszko, R. R. Whittle and H. R. Allcock, *J. Chem. Soc., Chem. Commun.*, 1982, 649–650.
25 V. Lavallo, Y. Canac, C. Prasang, B. Donnadieu and G. Bertrand, *Angew. Chem., Int. Ed.*, 2005, **44**, 5705–5709.
26 E. A. LaPierre, L. K. Watanabe, B. O. Patrick, J. M. Rawson, H. M. Tuononen and I. Manners, *J. Am. Chem. Soc.*, 2023, **145**, 9223–9232.
27 E. A. LaPierre, B. O. Patrick and I. Manners, *J. Am. Chem. Soc.*, 2024, **146**, 6326–6335.
28 Y. Wang and G. H. Robinson, *J. Am. Chem. Soc.*, 2023, **145**, 5592–5612.
29 D. Munz, *Organometallics*, 2018, **37**, 275–289.
30 S. Kumar Kushvaha, A. Mishra, H. W. Roesky and K. Chandra Mondal, *Chem.–Asian J.*, 2022, **17**, e202101301.
31 A. K. Eckhardt, M. Y. Riu, M. Ye, P. Muller, G. Bistoni and C. C. Cummins, *Nat. Chem.*, 2022, **14**, 928–934.
32 C. Hering, A. Schulz and A. Villinger, *Chem. Sci.*, 2014, **5**, 1064–1073.
33 R. Kinjo, B. Donnadieu and G. Bertrand, *Angew. Chem., Int. Ed.*, 2010, **49**, 5930–5933.
34 E. Niecke, M. Nieger and F. Reichert, *Angew. Chem., Int. Ed.*, 2003, **27**, 1715–1716.
35 J. L. Martinez, S. A. Lutz, D. M. Beagan, X. Gao, M. Pink, C. H. Chen, V. Carta, P. Moenne-Loccoz and J. M. Smith, *ACS Cent. Sci.*, 2020, **6**, 1572–1577.
36 A. K. Eckhardt, M. Y. Riu, P. Muller and C. C. Cummins, *Inorg. Chem.*, 2022, **61**, 1270–1274.
37 A. Velian and C. C. Cummins, *Science*, 2015, **348**, 1001–1004.
38 R. Ahlrichs, M. Bär, H. S. Plitt and H. Schnöckel, *Chem. Phys. Lett.*, 1989, **161**, 179–184.
39 I. K. Ahmad and P. A. Hamilton, *J. Mol. Spectrosc.*, 1995, **169**, 286–291.
40 J. Curry, L. Herzberg and G. Herzberg, *J. Chem. Phys.*, 1933, **1**, 749.
41 J. Curry, L. Herzberg and G. Herzberg, *Z. Phys.*, 1933, **86**, 348–366.
42 A. A. Starikova, N. M. Boldyreva, R. M. Minyaev, A. I. Boldyrev and V. I. Minkin, *ACS Omega*, 2018, **3**, 286–291.
43 F. C. Wyse, W. Gordy and E. L. Manson, *J. Chem. Phys.*, 1972, **57**, 1106.
44 R. M. Atkins and P. L. Timms, *Inorg. Nucl. Chem. Lett.*, 1978, **14**, 113–115.
45 C. Zhu, A. K. Eckhardt, A. Bergantini, S. K. Singh, P. R. Schreiner and R. I. Kaiser, *Sci. Adv.*, 2020, **6**, eaba6934.
46 C. Zhu, A. K. Eckhardt, S. Chandra, A. M. Turner, P. R. Schreiner and R. I. Kaiser, *Nat. Commun.*, 2021, **12**, 5467.
47 D. Tofan and A. Velian, *ACS Cent. Sci.*, 2020, **6**, 1485–1487.
48 B. E. Turner and J. Bally, *Astrophys. J.*, 1987, **321**, L75.
49 S. Roy, K. C. Mondal, S. Kundu, B. Li, C. J. Schurmann, S. Dutta, D. Koley, R. Herbst-Irmer, D. Stalke and H. W. Roesky, *Chem.–Eur. J.*, 2017, **23**, 12153–12157.
50 C. Adamo and V. Barone, *J. Chem. Phys.*, 1999, **110**, 6158–6170.
51 F. Weigend and R. Ahlrichs, *Phys. Chem. Chem. Phys.*, 2005, **7**, 3297–3305.
52 S. Grimme, S. Ehrlich and L. Goerigk, *J. Comput. Chem.*, 2011, **32**, 1456–1465.
53 S. W. Bartlett, S. J. Coles, D. B. Davies, M. B. Hursthouse, H. Ibisoglu, A. Kilic, R. A. Shaw and I. Un, *Acta Crystallogr., Sect. B*, 2006, **62**, 321–329.
54 J. Tomasi, B. Mennucci and R. Cammi, *Chem. Rev.*, 2005, **105**, 2999–3093.
55 K. B. Wiberg, *Tetrahedron*, 1968, **24**, 1083–1096.
56 J. Meija, T. B. Coplen, M. Berglund, W. A. Brand, P. De Bièvre, M. Gröning, N. E. Holden, J. Irrgeher, R. D. Loss, T. Walczyk and T. Prohaska, *Pure Appl. Chem.*, 2016, **88**, 293–306.
57 D. W. Allen and B. F. Taylor, *J. Chem. Soc., Dalton Trans.*, 1982, 51–54.
58 U. Beckmann, D. Süslüyan and P. C. Kunz, *Phosphorus, Sulfur Silicon Relat. Elem.*, 2011, **186**, 2061–2070.
59 G. P. Junor, J. Lorkowski, C. M. Weinstein, R. Jazzar, C. Pietraszuk and G. Bertrand, *Angew. Chem., Int. Ed.*, 2020, **59**, 22028–22033.
60 P. W. Codding and K. A. Kerr, *Acta Crystallogr., Sect. B*, 1978, **34**, 3785–3787.
61 P. W. Codding and K. A. Kerr, *Acta Crystallogr., Sect. B*, 1979, **35**, 1261–1263.
62 P. Perez-Galan, N. Delpont, E. Herrero-Gomez, F. Maseras and A. M. Echavarren, *Chem.–Eur. J.*, 2010, **16**, 5324–5332.
63 R. Dorel and A. M. Echavarren, *Chem. Rev.*, 2015, **115**, 9028–9072.
64 L. Falivene, Z. Cao, A. Petta, L. Serra, A. Poater, R. Oliva, V. Scarano and L. Cavallo, *Nat. Chem.*, 2019, **11**, 872–879.

Open Access Article. Published on 24 April 2025. Downloaded on 2/22/2026 5:57:45 PM.
This article is licensed under a Creative Commons Attribution-NonCommercial 3.0 Unported Licence.

65 H. Clavier and S. P. Nolan, *Chem. Commun.*, 2010, **46**, 841–861.
66 A. R. Chianese, X. Li, M. C. Janzen, J. W. Faller and R. H. Crabtree, *Organometallics*, 2003, **22**, 1663–1667.
67 L. Perrin, E. Clot, O. Eisenstein, J. Loch and R. H. Crabtree, *Inorg. Chem.*, 2001, **40**, 5806–5811.
68 T. D. Tilley, R. H. Grubbs and J. E. Bercaw, *Organometallics*, 1984, **3**, 274–278.
69 B. K. Campion, R. H. Heyn and T. D. Tilley, *J. Chem. Soc., Chem. Commun.*, 1988, 278–280.
70 P. J. Fagan, M. D. Ward and J. C. Calabrese, *J. Am. Chem. Soc.*, 1989, **111**, 1698–1719.
71 J. M. Herbert, *Phys. Chem. Chem. Phys.*, 2024, **26**, 3755–3794.
72 T. Le Bahers, C. Adamo and I. Ciofini, *J. Chem. Theory Comput.*, 2011, **7**, 2498–2506.
73 C. Adamo, T. Le Bahers, M. Savarese, L. Wilbraham, G. García, R. Fukuda, M. Ehara, N. Rega and I. Ciofini, *Coord. Chem. Rev.*, 2015, **304**, 166–178.
74 H. Tsurugi and K. Mashima, *Acc. Chem. Res.*, 2019, **52**, 769–779.
75 W. Kaim, *J. Am. Chem. Soc.*, 1983, **105**, 707–713.
76 L. Jafarpour, E. D. Stevens and S. P. Nolan, *J. Organomet. Chem.*, 2000, **606**, 49–54.
77 P. Pyykko, *J. Phys. Chem. A*, 2015, **119**, 2326–2337.
78 P. Pyykkö and M. Atsumi, *Chem.–Eur. J.*, 2009, **15**, 12770–12779.
79 C. C. Levin, *J. Am. Chem. Soc.*, 1975, **97**, 5649–5655.
80 I. Manners, H. R. Allcock, G. Renner and O. Nuyken, *J. Am. Chem. Soc.*, 1989, **111**, 5478–5480.
81 J. A. Dodge, I. Manners, H. R. Allcock, G. Renner and O. Nuyken, *J. Am. Chem. Soc.*, 1990, **112**, 1268–1269.
82 M. Liang and I. Manners, *J. Am. Chem. Soc.*, 1991, **113**, 4044–4045.
83 E. Niecke and W. Bitter, *Inorg. Nucl. Chem. Lett.*, 1973, **9**, 127–129.
84 B. Wang, E. Rivard and I. Manners, *Inorg. Chem.*, 2002, **41**, 1690–1691.
85 C. H. Honeyman, I. Manners, C. T. Morrissey and H. R. Allcock, *J. Am. Chem. Soc.*, 1995, **117**, 7035–7036.
86 H. R. Allcock, C. A. Crane, C. T. Morrissey, J. M. Nelson, S. D. Reeves, C. H. Honeyman and I. Manners, *Macromolecules*, 1996, **29**, 7740–7747.

© 2025 The Author(s). Published by the Royal Society of Chemistry